Velocity fluctuations in a dilute suspension of viscous vortex rings

Thomas A. Morrell,* Saverio E. Spagnolie,† and Jean-Luc Thiffeault‡
Department of Mathematics, University of Wisconsin–Madison, 480 Lincoln Drive, Madison, Wisconsin 53706, USA

(Received 4 September 2018; published 8 April 2019)

We explore the velocity fluctuations in a fluid due to a dilute suspension of randomly distributed vortex rings at moderate Reynolds number, for instance, those generated by a large colony of jellyfish. Unlike previous analysis of velocity fluctuations associated with gravitational sedimentation or suspensions of microswimmers, here the vortices have a finite lifetime and are constantly being produced. We find that the net velocity distribution is similar to that of a single vortex, except for the smallest velocities which involve contributions from many distant vortices; the result is a truncated 5/3-stable distribution with variance (and mean energy) linear in the vortex volume fraction ϕ. The distribution has an inner core with a width scaling as $\phi^{3/5}$, then long tails with power law $|u|^{-8/3}$, and finally a fixed cutoff (independent of ϕ) above which the probability density scales as $|u|^{-5}$, where u is a component of the velocity. We argue that this distribution is robust in the sense that the distribution of any velocity fluctuations caused by random forces localized in space and time has the same properties, except possibly for a different scaling after the cutoff.

DOI: 10.1103/PhysRevFluids.4.044501

I. INTRODUCTION

A natural question when faced with a fluid flow with some degree of randomness is how to characterize its velocity fluctuations. This is a classical problem in turbulence but also in gravitational sedimentation [1–6] and in suspensions of microswimmers [7–19]. In the case of sedimentation and microswimmers, the velocity field due to a single particle or swimmer is commonly used as a building block to understand the velocity distribution in the full system. At leading order for a dilute suspension, interactions are neglected and much is learned by examining a random superposition of individual particles or swimmers. In particular, for small velocities the distribution is typically Gaussian [19], since superimposing many distant sources usually results in an application of the central limit theorem.

In this paper we study the velocity distribution in a dilute suspension of viscous vortex rings. We assume some mechanism, such as a colony of jellyfish, generates vortices randomly throughout time and space, as observed and illustrated in Fig. 1. These vortices decay due to viscosity but are replenished such that the system is assumed to reach a statistical equilibrium, containing vortices with some age distribution. Turbulence has been modeled with some success using vortex rings [20–22], but here we investigate a moderate Reynolds number regime which is still a long way from turbulence (the jellyfish are assumed to be a few centimeters in size so that the rings they generate are strongly affected by viscosity). Other related biological systems may also exhibit related velocity field fluctuations that may have important functional consequences. In particular, nonmotile pulsing

*tamorrell@math.wisc.edu
†spagnolie@math.wisc.edu
‡jeanluc@math.wisc.edu

FIG. 1. (Left) A "suspension" of spotted jellyfish (*Mastigias papua*) at the Vancouver Aquarium. (Center) Fast swimming *Nemopsis bachei* expels a single vortex ring with each rapid pulse (reproduced with permission from [41]). (Right) Schematic of the problem: we seek the distribution of the fluid velocity $\boldsymbol{u}$ at $\boldsymbol{r}_0$ due to a randomly distributed suspension of viscous vortex rings in three dimensions.

corals share considerable hydrodynamic similarities with undulating jellyfish, and their repeated pulsing is known to contribute to fluid mixing, nutrient transport, and the rate of photosynthesis at intermediate Reynolds numbers [23–25]. A better understanding of the velocity fluctuations in suspensions may also be of use in the design of biomimetic systems for related purposes [26–28],

One key to developing analytical estimates for velocity fluctuations is to start with a tractable "building block," in this case a simple model for a vortex ring. There exists a great wealth of literature containing analytical, numerical, and experimental results for vortex rings [29–40], but to study the role of viscous vortex decay, a classical ideal vortex model is insufficient. Instead, we shall use an intermediate-Reynolds number model of a decaying vortex ring due to Fukumoto and Kaplanski [35].

In the following pages we show analytically and verify numerically that the probability distribution for the velocity fluctuations of a dilute suspension of vortex rings is a truncated 5/3-stable distribution. Recall that a distribution is stable if it is invariant under summation of independent random variables (with the given distribution), up to location and scaling. The standard symmetric α-stable distribution has the form

$$\Phi_\alpha(u;a) = \frac{1}{2\pi}\int_{-\infty}^{\infty} e^{iku-a|k|^\alpha}\,dk \tag{1}$$

for $0 < \alpha \leqslant 2$. The 2-stable distribution is a Gaussian, while for $\alpha < 2$, the distribution has infinite variance and is tail-heavy:

$$\Phi_\alpha(u;a) \sim \frac{a\Gamma(\alpha+1)}{\pi|u|^{\alpha+1}}\sin\left(\frac{\pi\alpha}{2}\right) \tag{2}$$

as $|u| \to \infty$ [18,42,43]. For a truncated stable distribution, the $|u|^{-\alpha-1}$ tails only persist up to some finite value of $|u|$, with a faster decay beyond the cutoff, similar to Min *et al.* [44]. These results are robust in the sense that any flow produced by impulses sufficiently localized in both space and time will produce the same velocity distribution. The variance of u (mean energy) is shown to be linear in the vortex volume fraction ϕ as expected from such a superposition of individual velocity fields. However, the width of the core scales as $\phi^{3/5}$ rather than $\phi^{1/2}$, suggesting that the tails of the distribution contribute at leading-order to the energy.

The paper is structured as follows. In Sec. II, we present a model of a viscous vortex ring due to Fukumoto and Kaplanski [35]. In Sec. III, we build a suspension of viscous vortices by superimposing the flow fields of individual model vortex rings, and we subsequently derive an estimate for the energy of the suspension. This analysis is expanded in Sec. IV to determine the full velocity distribution analytically. These findings are confirmed numerically using simulations involving the evaluation of transient velocity fields over multiple scales. We show in Sec. V that under a particular set of conditions, the $|u|^{-8/3}$ power law observed in the distribution is robust and is a consequence of swimming occurring in a three-dimensional fluid. Concluding remarks are given in Sec. VI.

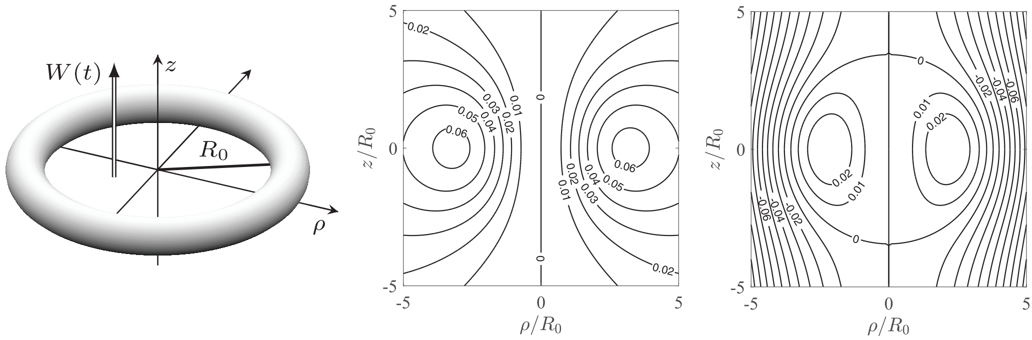

FIG. 2. (Left) Diagram of an early-stage vortex ring. (Center) Contours of the streamfunction Ψ normalized by $\Gamma_0 R_0$ in the laboratory frame from Eq. (4b) at time $t = R_0^2/\nu$. (Right) The same normalized streamfunction in a frame moving with the vortex ring.

II. A SINGLE VISCOUS VORTEX RING

Before analyzing a suspension of vortices, we start by presenting a model of a single viscous vortex ring due to Fukumoto and Kaplanski [35]. They consider the case of an axisymmetric vortex filament with initial azimuthal vorticity,

$$\zeta(\rho, z, t = 0) = \Gamma_0\, \delta(z)\, \delta(\rho - R_0), \tag{3}$$

where δ is the Dirac δ function, Γ_0 is the initial circulation, R_0 is the initial radius of the vortex ring, ρ and z are the radial and axial directions in space relative to the vortex ring (see the diagram in Fig. 2), and t is time. In this setting it is convenient to define a stream function $\Psi(\rho, z, t)$, where the velocity in the laboratory frame is given by $\boldsymbol{v} = \rho^{-1}\, \nabla^{\perp}\Psi$, with $\nabla^{\perp} = \hat{z}\,\partial_\rho - \hat{\rho}\,\partial_z$. Defining the Reynolds number as $\mathrm{Re} := \Gamma_0/\nu$, where ν is the kinematic viscosity, Fukumoto and Kaplanski [35] find that the swirl-free flow, to leading order in small Reynolds number with initial condition Eq. (3), takes the form

$$\zeta(\rho, z, t) = \frac{\Gamma_0 R_0}{4\sqrt{\pi}(\nu t)^{3/2}} \exp\left(-\frac{z^2 + \rho^2 + R_0^2}{4\nu t}\right) I_1\left(\frac{R_0 \rho}{2\nu t}\right), \tag{4a}$$

$$\Psi(\rho, z, t) = \frac{1}{4}\Gamma_0 R_0 \rho \int_0^\infty \left[e^{mz}\, \mathrm{erfc}\left(\frac{2m\nu t + z}{2\sqrt{\nu t}}\right) + e^{-mz}\, \mathrm{erfc}\left(\frac{2m\nu t - z}{2\sqrt{\nu t}}\right)\right] J_1(mR_0) J_1(m\rho)\, dm. \tag{4b}$$

Here J_1 and I_1 are standard and modified Bessel functions of the first kind, respectively, and erfc is the complementary error function. The circulation is found to decay in time as $\Gamma(t) = \Gamma_0[1 - \exp(-R_0^2/4\nu t)]$. A useful approximation to Ψ is

$$\Psi(\rho, z, t) \approx \frac{\Gamma_0 R_0^2}{2\sqrt{\pi}} \left(\int_0^\xi e^{-\xi'^2}\, d\xi' - \xi\, e^{-\xi^2}\right) \frac{\rho^2}{(z^2 + \rho^2)^{3/2}}, \qquad \frac{R_0}{\sqrt{4\nu t}} \ll \max(\xi, 1), \tag{5}$$

where

$$\xi(\rho, z, t) := \sqrt{(z^2 + \rho^2)/4\nu t} \tag{6}$$

is a dimensionless measure of the position relative to the "viscous front" at $\xi = 1$ associated with the outward propagation of viscous stresses, which are only significant at the boundary between the growing vortex ring and the surrounding fluid. Crucially, the form of Eq. (5) is valid even at small t, as long as we are considering points well outside the vortex ring. Applying small and large ξ

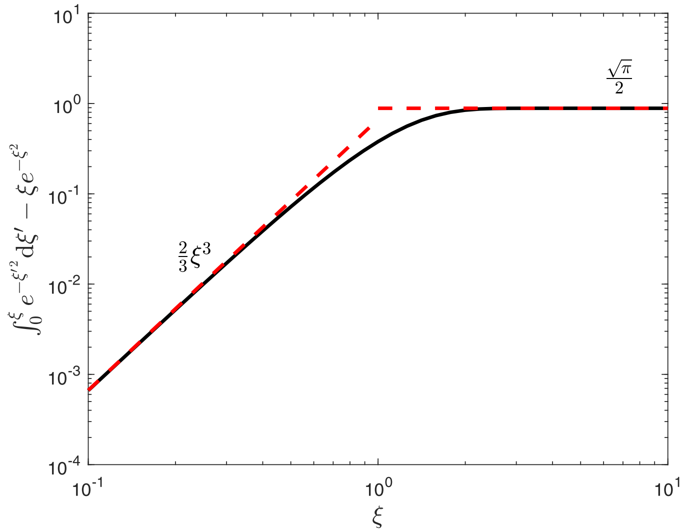

FIG. 3. Plot of the terms involving ξ inside the parentheses of Eq. (5), along with the small and large ξ approximations used to derive Eq. (7). We see that the approximations are very good outside of a transition region with $0.4 \lesssim \xi \lesssim 2.5$.

approximations to Eq. (5), we find an approximate velocity field

$$\boldsymbol{v}(\rho, z, t) = \begin{cases} \frac{\Gamma_0 R_0^2 \hat{\boldsymbol{z}}}{12\sqrt{\pi}(\nu t)^{3/2}} & \xi \lesssim 1, \\ \frac{\Gamma_0 R_0^2[(2z^2-\rho^2)\hat{\boldsymbol{z}}+3z\rho\,\hat{\boldsymbol{\rho}}]}{4(z^2+\rho^2)^{5/2}} & \xi \gtrsim 1, \end{cases} \qquad \frac{R_0}{\sqrt{4\nu t}} \ll \max(\xi, 1), \tag{7}$$

with a relatively sharp transition region around the viscous front $\xi = 1$. Note that although the two parts of Eq. (7) were derived in the asymptotic regimes where $\xi \ll 1$ and $\xi \gg 1$, respectively, they are good approximations for most points (see Fig. 3), except for at small times and in an annulus surrounding the viscous front $0.4 \lesssim \xi \lesssim 2.5$. Note that the large ξ approximation matches the flow for an inviscid vortex ring, while fluid inside the vortex ring mostly moves uniformly, so viscous stresses are only significant in this transition region.

The vortex ring also propels itself forward in time. To find the self-advection of the vortex ring and incorporate it into the model, Fukumoto and Kaplanski use the Helmholtz–Lamb transformation, from which they determine the instantaneous speed $W(t)$ of the vortex ring and the net displacement $S(t)$ in the positive z direction [35]. Incorporating the vortex speed W into the streamfunction by subtracting $\frac{1}{2}\rho W^2$ from Ψ results in the more familiar ellipsoidal envelope corresponding to $\Psi = 0$ as shown in Fig. 2 (right).

The model matches previous estimates for the early and late time velocities [30,33,45]. Fukumoto and Kaplanski [35] also validate their model against experimental results from Cater *et al.* [34] with Re = 2000 and find excellent agreement, suggesting Eq. (4) accurately captures the structure of the fluid flow for a broad range of intermediate Reynolds numbers, including those of various jellyfish [46–48]. For the *Aurelia aurita* jellyfish in a Danish fjord studied by Olesen *et al.* [49], we can estimate that Re ranges from around 60 to 2160.

The model has a finite second moment (i.e., finite energy). Fukumoto and Kaplanski [35] find that the energy in the entire fluid at a time t is given by

$$E_1(t) = \frac{1}{2}\int_V |\boldsymbol{v}|^2 \, dV = \frac{\sqrt{\pi}\,\Gamma_0^2 R_0^4}{48\sqrt{2}(\nu t)^{3/2}}\, {}_2F_2\!\left(\frac{3}{2}, \frac{3}{2}; \frac{5}{2}, 3; -\frac{R_0^2}{2\nu t}\right), \tag{8}$$

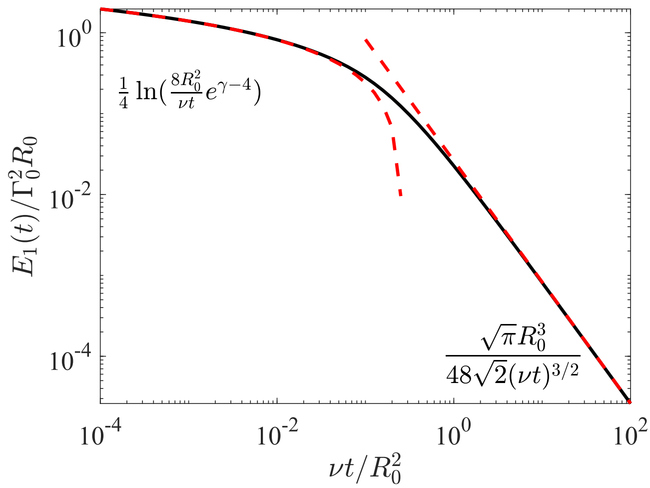

FIG. 4. The energy integrated over all space $E_1(t)$ for a single vortex ring normalized by $\Gamma_0^2 R_0$ and compared with the small and large-time asymptotics in Eq. (9).

where ${}_2F_2$ is a generalized hypergeometric function. This has asymptotic forms

$$E_1(t) \sim \begin{cases} \Gamma_0^2 R_0\left(\frac{1}{4}\ln(8R_0^2/\nu t) + \frac{1}{4}\gamma - 1\right), & \text{as } t \downarrow 0, \\ \frac{\sqrt{\pi}\,\Gamma_0^2 R_0^4}{48\sqrt{2}(\nu t)^{3/2}}, & \text{as } t \to \infty, \end{cases} \tag{9}$$

where γ is the Euler–Mascheroni constant. These asymptotic forms are plotted in Fig. 4 to indicate their degree of accuracy when compared to E_1. Remarkably, $E_1(t)$ can be integrated over time exactly, to obtain the total vortex action

$$\mathcal{E}_1 := \int_0^\infty E_1(t)\, dt = \frac{\Gamma_0^2 R_0^3}{6\nu} = \frac{1}{6}\mathrm{Re}^2\, \nu R_0^3. \tag{10}$$

A discussion of other moments of the velocity integrated over space and time can be found in Appendix A. In particular, the moments M_n are only finite when $\frac{5}{3} < n < 4$.

III. ENERGY OF A SUSPENSION OF VISCOUS VORTICES

In this section we find an analytical estimate for the energy of a suspension of viscous vortices, which will be used in the analysis of the full velocity distribution. Vortex rings are assumed to come into being uniformly in time, space, and orientation, into an otherwise quiescent infinite bath. The rate of vortex production is μ vortices per unit time per unit volume, which when nondimensionalized becomes an effective volume fraction $\phi := \mu R_0^5/\nu$. Since vortices decay over time, there is a natural correspondence between vortex production and volume fraction. Note that with a high enough rate of production, ϕ can be greater than one. This is not unphysical, as vortices can overlap.

In nature, concentrations *Aurelia aurita* jellyfish have been observed in the range of 1×10^{-6} to 3×10^{-4} medusae per cubic centimeter with mean radius R_0 ranging from 0.125 to 2.7 cm depending on the time of year [49]. Meanwhile, McHenry and Jed [46] found that jellyfish pulsed at a rate of once per second for smaller medusae, and once per two seconds for larger medusae. We therefore estimate that, for the suspension of vortices, ϕ ranges from 3×10^{-8} in early spring to 0.3 in late summer. Thus, we will assume that $\phi \ll 1$, and therefore that any vortex-vortex interactions are negligible.

Consider the velocity field $\boldsymbol{v}(\boldsymbol{r},t) = \rho^{-1}\,\nabla^{\perp}\Psi$, with $\nabla^{\perp} = \hat{z}\,\partial_\rho - \hat{\rho}\,\partial_z$, for a vortex initially at the origin and pointing in the $\hat{z}$ direction as in Fig. 2. Rotating and translating the velocity to represent a vortex with arbitrary position and direction, we first obtain the rotated velocity field

$$\mathbb{Q}\cdot\boldsymbol{v}(\mathbb{Q}^{-1}\cdot\boldsymbol{r},t), \tag{11}$$

where $\mathbb{Q}$ is a rotation matrix, and then translate the field to point $\boldsymbol{R}$ (replacing $\boldsymbol{r}$ by $\boldsymbol{r}-\boldsymbol{R}$):

$$\mathbb{Q}\cdot\boldsymbol{v}(\mathbb{Q}^{-1}\cdot(\boldsymbol{r}-\boldsymbol{R}),t). \tag{12}$$

Writing the vortex position in time as

$$\boldsymbol{R}(t) = \boldsymbol{R}(0) + S(t)\,\mathbb{Q}\cdot\hat{z}, \qquad S(0)=0, \tag{13}$$

[recall that $S(t)$ is the vortex displacement and $W(t)=S'(t)$ is the speed], thus results in its induced velocity field

$$\mathbb{Q}\cdot\boldsymbol{v}(\mathbb{Q}^{-1}\cdot(\boldsymbol{r}-\boldsymbol{R}(0)) - \hat{z}S(t),\ t). \tag{14}$$

Summing the velocity contributions at a point $\boldsymbol{r}_0$ from N independent vortices, which are initially located at random points $\boldsymbol{R}_k$, results in

$$\boldsymbol{U} = \sum_{k=1}^{N}\mathbb{Q}_k\cdot\boldsymbol{v}\big(\mathbb{Q}_k^{-1}\cdot(\boldsymbol{r}_0-\boldsymbol{R}_k) - \hat{z}\,S(T_k),T_k\big), \tag{15}$$

where the random variable T_k denotes the age of the kth vortex, and $\mathbb{Q}_k$ is a random rotation matrix, which enforces isotropy. We assume $N=\mu V\tau$ is constant, where V is the total volume of the domain and τ is the lifetime of a vortex. Here, V,τ are assumed finite, but we will examine the infinite volume and time limits shortly.

The expected value of $\boldsymbol{U}$, $\langle\boldsymbol{U}\rangle$, averaged over all positions, orientations, and birth times, is

$$\langle\boldsymbol{U}\rangle = N\int_\Omega\int_0^\tau\int_V \mathbb{Q}\cdot\boldsymbol{v}(\mathbb{Q}^{-1}(\Omega)\cdot(\boldsymbol{r}_0-\boldsymbol{r}) - \hat{z}\,S(t),\ t)\,\frac{dV_{\boldsymbol{r}}}{V}\,\frac{dt}{\tau}\,\frac{d\Omega}{4\pi}, \tag{16}$$

with Ω the solid angle that determines the rotation matrix. With the change of variables

$$\boldsymbol{r}' = \mathbb{Q}^{-1}(\Omega)\cdot(\boldsymbol{r}_0-\boldsymbol{r}) - \hat{z}\,S(t), \quad t'=t, \tag{17}$$

we have $\partial\boldsymbol{r}'/\partial\boldsymbol{r} = -\mathbb{Q}^{-1}(\Omega)$, and $\partial\boldsymbol{r}'/\partial t = -W(t)\hat{z}$. The Jacobian matrix for the transformation is

$$\frac{\partial(\boldsymbol{r}',t')}{\partial(\boldsymbol{r},t)} = \begin{pmatrix} -\mathbb{Q}^{-1}(\Omega) & -W(t)\hat{z} \\ 0 & 1\end{pmatrix}, \tag{18}$$

with determinant -1, so the Jacobian does not modify the integral:

$$\langle\boldsymbol{U}\rangle = N\int_\Omega\int_0^\tau\int_{V'(\boldsymbol{r}_0,t',\Omega)}\mathbb{Q}\cdot\boldsymbol{v}(\boldsymbol{r}',t')\,\frac{dV_{\boldsymbol{r}'}}{V}\,\frac{dt'}{\tau}\,\frac{d\Omega}{4\pi}. \tag{19}$$

Here $V'(\boldsymbol{r}_0,t',\Omega)$ is the domain of integration transformed according to Eq. (17).

Similarly, the qth absolute moment of $\boldsymbol{U}$ can be computed as

$$\langle|\boldsymbol{U}|^q\rangle = N\int_\Omega\int_0^\tau\int_V|\boldsymbol{v}(\boldsymbol{r}',t')|^q\,\frac{dV_{\boldsymbol{r}'}}{V}\,\frac{dt'}{\tau}\,\frac{d\Omega}{4\pi}. \tag{20}$$

Integrating over the orientation angles and dropping the primes,

$$\langle|\boldsymbol{U}|^q\rangle = N\int_0^\tau\int_V|\boldsymbol{v}(\boldsymbol{r},t)|^q\,\frac{dV_{\boldsymbol{r}}}{V}\,\frac{dt}{\tau} = \mu\int_0^\tau\int_V|\boldsymbol{v}(\boldsymbol{r},t)|^q\,dV_{\boldsymbol{r}}\,dt. \tag{21}$$

Setting $q = 2$, taking $V = \mathbb{R}^3$ and $\tau \to \infty$ (and dividing by two), we find the expectation of the energy

$$\langle E \rangle = \frac{1}{2}\mu \int_0^\tau \int_V |\boldsymbol{v}(\boldsymbol{r},t)|^2 \, dV_{\boldsymbol{r}} \, dt = \mu \mathcal{E}_1 = \frac{\phi}{6} \frac{\Gamma_0^2}{R_0^2}. \tag{22}$$

Thus, the expected energy is μ times Eq. (10), the energy of a single vortex integrated over time and space. This is reasonable: In this noninteracting dilute limit, the energy of the system is the sum of the energies of the individual vortices.

IV. VELOCITY DISTRIBUTION

A more refined analysis than that of Sec. III allows us to characterize the entire velocity distribution, rather than just the moments. This clarifies whether the dominant contribution to the moments arises from near or far field dynamics, as well as facilitating potential comparisons to experiments. For small concentrations, we will find stable distributions similar to Zaid *et al.* [17] or Zaid and Mizuno [18] for suspensions of microswimmers, though the relationship between spatial velocity decay and the tail exponents is modified here by the additional temporal behavior of the vortices.

A. Single vortex

We first consider the velocity distribution due to a single vortex ring, which will be used in Sec. IV B to derive the marginal distribution for the velocity fluctuations in a suspension of viscous vortices. We choose a random point $\boldsymbol{r} = \boldsymbol{r}_0 + (\rho\cos\theta, \rho\sin\theta, z)$ uniformly inside the ball $V = B_L(\boldsymbol{r}_0)$ of radius L centered at $\boldsymbol{r}_0$, and choose a random vortex age t uniformly in $[0, \tau]$. The probability density function $p_{U^1}(u)$ for the magnitude of the single-vortex velocity $U^1 = |\boldsymbol{U}^1|$ is

$$p_{U^1}(u) = \int_0^\tau \int_V \delta(u - v(\boldsymbol{r},t)) \frac{dV_{\boldsymbol{r}}}{V} \frac{dt}{\tau}, \tag{23}$$

where $v(\boldsymbol{r},t) = |\boldsymbol{v}(\boldsymbol{r},t)|$. The δ function constrains the integral to a hypersurface $v(\boldsymbol{r},t) = u$:

$$p_{U^1}(u) = \frac{1}{V\tau} \int_{v(\boldsymbol{r},t)=u} \frac{1}{|\boldsymbol{\nabla}_{(\boldsymbol{r},t)} v(\boldsymbol{r},t)|} \, dS_{\boldsymbol{r},t}, \tag{24}$$

where $|\boldsymbol{\nabla}_{(\boldsymbol{r},t)} v(\boldsymbol{r},t)|$ is a Jacobian [50] and $dS_{\boldsymbol{r},t}$ is the integration element on the hypersurface $v(\boldsymbol{r},t) = u$. An analytical estimate may be achieved by splitting the integral into two pieces, $\xi \leqslant 1$ and $\xi \geqslant 1$ with $\xi = |\boldsymbol{r}|/\sqrt{4\nu t}$, and using Eq. (7), valid for small u, to approximate the velocity. (We neglect the transition region near $\xi = 1$.) This straightforward but somewhat messy calculation is carried out in Appendix B. By combining Eqs. (B1) and (B4), we find that

$$p_{U^1}(u) \lesssim \frac{0.1514}{V\tau} \frac{\Gamma_0^{5/3} R_0^{10/3}}{\nu} u^{-8/3}, \quad \varepsilon \ll \frac{uR_0}{\Gamma_0} \ll 1, \tag{25}$$

where

$$\varepsilon = \frac{R_0^3}{\min[V, (\nu\tau)^{3/2}]}. \tag{26}$$

The approximation breaks down as $(uR_0/\Gamma_0) \uparrow 1$ because then the details of the near field of the vortex become important, and we cannot use Eq. (7) to go from Eq. (24) to (25) as we did above. The approximation Eq. (25) also breaks down as $(uR_0/\Gamma_0) \downarrow \varepsilon$ because, at fixed V and τ, the region $v(\boldsymbol{r},t) < \varepsilon\Gamma_0/R_0$ falls outside the domain of integration in Eq. (23). The value of ε is typically small, indicating a wide range of validity for Eq. (25), as long as the domain radius L is much larger than the vortex size R_0, and the time of integration τ is much longer than the viscous dissipation time R_0^2/ν.

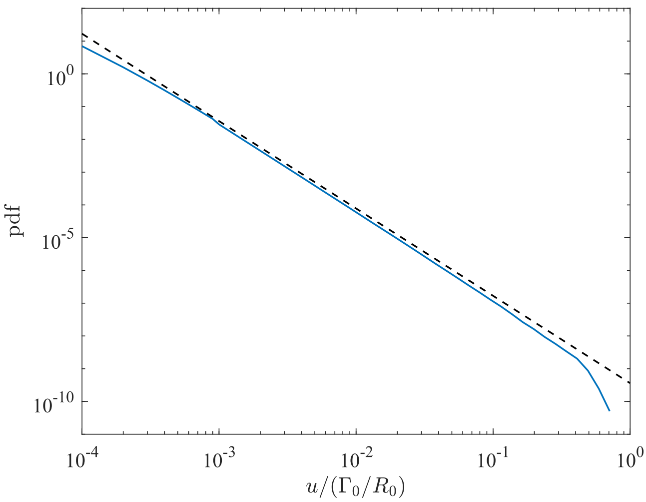

FIG. 5. The numerically evaluated velocity probability density function for a single vortex ring (solid line) compared with the analytic approximation Eq. (25) (dashed line). The approximation is about 40% higher than the numerical values on the segment with $0.001\Gamma_0/R_0 \lesssim u \lesssim 0.04\Gamma_0/R_0$.

To probe the accuracy of this approximation, we computed Eq. (23) via Monte Carlo integration, finding the velocity at a point $\boldsymbol{r}_0$ using a second-order finite difference approximation of Eq. (4b) for a single vortex ring (see Sec. IV C for more details) positioned randomly in $B_L(\boldsymbol{r}_0)$ with $\Gamma_0 = 100\nu$, $L = 100\,R_0$, and $\tau = 100\,R_0^2/\nu$, and continuing to sample until the distribution converged. Figure 5 shows a comparison between the numerical computation of Eq. (23) and the analytical approximation Eq. (25). We see that the $u^{-8/3}$ power law holds over a wide range of values of u. The analytical prediction Eq. (25) is about 40% too large when compared with the numerics due to the transition region around $\xi \approx 1$. However, this error does not affect the exponent in the $-8/3$ power law, just the prefactor.

B. Suspension of vortices

We now use the velocity distribution for a single vortex ring to determine the corresponding distribution for a suspension of vortices, modifying the argument of Thiffeault [51] that characterized the drifts associated with microswimmers. We will use components of the velocity instead of its magnitude, since components can be added together but not magnitudes. This additivity of velocity is a good approximation at low volume fractions ϕ. Since we have assumed isotropy of the suspension, there is no loss in generality in considering only a single component of the fluid velocity $\boldsymbol{u}$.

Starting from the single-vortex distribution $p_{U^1}(u)$ for the magnitude of velocity, Eq. (23), we convert to the distribution for the components with

$$p_{\boldsymbol{U}^1}(\boldsymbol{u}) = p_{\boldsymbol{U}^1}(\boldsymbol{u}|u)\,p_{U^1}(u) = \int_V \int_0^\tau \frac{\delta(u - v(\boldsymbol{r},t))}{4\pi u^2}\,\frac{dt}{\tau}\,\frac{dV_{\boldsymbol{r}}}{V}, \qquad u = |\boldsymbol{u}|, \tag{27}$$

where, due to the isotropy of $\boldsymbol{u}$, $p_{\boldsymbol{U}^1}(\boldsymbol{u}|u) = 1/4\pi u^2$ is the uniform distribution on the sphere of radius u. We then find the marginal distribution for the x component of $\boldsymbol{u}$, denoted by u_x:

$$p_{U_x^1}(u_x) = \int_{-\infty}^{\infty}\int_{-\infty}^{\infty} p_{\boldsymbol{U}^1}(\boldsymbol{u})\,du_y\,du_z = \int_V \int_0^\tau \int_{-\infty}^{\infty}\int_{-\infty}^{\infty} \frac{\delta(u - v(\boldsymbol{r},t))}{4\pi u^2}\,du_y\,du_z\,\frac{dt}{\tau}\,\frac{dV_{\boldsymbol{r}}}{V}, \tag{28}$$

where the superscript 1 on U_x^1 and $\boldsymbol{U}^1$ is a reminder that this is still for a single vortex. Carrying out the integrals over u_y and u_z yields

$$p_{U_x^1}(u_x) = \int_V \int_0^\tau \frac{1}{2v(\boldsymbol{r}, t)} \left[v^2(\boldsymbol{r}, t) > u_x^2\right] \frac{dt}{\tau} \frac{dV_{\boldsymbol{r}}}{V}, \tag{29}$$

where $[A]$ is the indicator function of A, defined as 1 if A is true, and 0 otherwise.

To determine the distribution for multiple vortex rings, we compute the characteristic function

$$\left\langle e^{ikU_x^1}\right\rangle = \int_{-\infty}^{\infty} p_{U_x^1}(u_x)\, e^{iku_x}\, du_x = \int_V \int_0^\tau \operatorname{sinc}(kv(\boldsymbol{r}, t)) \frac{dt}{\tau} \frac{dV_{\boldsymbol{r}}}{V}, \tag{30}$$

where $\operatorname{sinc}(x) := \sin x/x$ for $x \neq 0$ and $\operatorname{sinc}(0) := 1$. We find that

$$\left\langle e^{ikU_x^1}\right\rangle = 1 - \frac{\gamma(k)}{V\tau}, \tag{31}$$

where

$$\gamma(k) := \int_V \int_0^\tau \{1 - \operatorname{sinc}(kv(\boldsymbol{r}, t))\}\, dt\; dV_{\boldsymbol{r}}. \tag{32}$$

Recall that μ is the constant rate of production of vortex rings, per unit space and time. Hence, after a time τ we have $N = \mu V\tau$ independent vortex rings, which together induce a random velocity U_x^N at the origin. The random variable U_x^N has characteristic function

$$\left\langle e^{ikU_x^N}\right\rangle = \left\langle e^{ikU_x^1}\right\rangle^N = \left(1 - \frac{\gamma(k)}{V\tau}\right)^{\mu V\tau} \sim \exp(-\mu\gamma(k)) \tag{33}$$

as $V, \tau \to \infty$ [51]. Therefore, for the suspension of vortices, the probability density function of velocities is obtained from the inverse Fourier transform

$$p_{U_x}(u_x) = \frac{1}{2\pi} \int_{-\infty}^{\infty} \exp(-\mu\gamma(k))\, e^{-iku_x}\, dk, \tag{34}$$

where we have dropped the superscript $N \to \infty$ on U_x.

Since $1 - \operatorname{sinc}(x) \sim \frac{1}{6}x^2$ as $x \to 0$, we have $\gamma(k) \sim \frac{1}{3}\mathcal{E}_1 k^2$ as $k \to 0$, from which we can solve for an approximate velocity distribution, mathematically valid as $\phi = \mu R_0^5/\nu \gg 1$:

$$p_{U_x}(u_x) \approx \sqrt{\frac{3}{4\pi\mu\mathcal{E}_1}} \exp\left(-\frac{3u_x^2}{4\mu\mathcal{E}_1}\right), \tag{35}$$

consistent with the central limit theorem. Then $\langle u_x^2\rangle = \frac{2}{3}\langle E\rangle = \frac{2}{3}\mu\mathcal{E}_1$, as predicted by Eq. (22). Recall that technically ϕ can be greater than one, since vortices can overlap. Of course, in the limit of large ϕ our linear superposition assumption breaks down, so Eq. (35) is unlikely to be observed in practice.

To find an approximation of the probability density function which is valid for small ϕ, where our model applies, we can use the probability distribution $p_{U^1}(u)$ from Eq. (25) to find an approximation of γ which is valid for large k in the limit as $V, \tau \to \infty$, by way of a change of variables to transform Eq. (32) into an integral over u:

$$\gamma(k) = V\tau \int_0^\infty \{1 - \operatorname{sinc}(ku)\}\, p_{U^1}(u)\, du \sim 0.1096\, \frac{\Gamma_0^{5/3} R_0^{10/3}}{\nu} |k|^{5/3} =: \frac{a}{\mu}|k|^{5/3} \tag{36}$$

[with $a = 0.1096\,\mu(\Gamma_0 R_0^2)^{5/3}/\nu = 0.1096\,(\Gamma_0/R_0)^{5/3}\phi$], where we have compensated for the uniform 40% overestimate of $p_{U^1}(u)$ by Eq. (25), as observed in Fig. 5 by decreasing the prefactor to match numerical estimates. We can compute Eq. (34) analytically using this γ; the result is a

$\frac{5}{3}$-stable distribution Eq. (1). For larger u_x, $\Phi_{5/3}(u_x;a)$ has tails

$$p_{U_x}(u_x) \sim \frac{1}{2\pi}\,\Gamma\!\left(\frac{8}{3}\right) a\,|u_x|^{-8/3}, \qquad \phi^{3/5} \ll \frac{u_x R_0}{\Gamma_0} \ll 1, \tag{37}$$

while for small u_x the core region is reasonably well approximated by a Gaussian

$$p_{U_x}(u_x) \sim 0.2844 a^{-3/5} \exp\left(-u_x^2/3.198 a^{6/5}\right), \qquad \frac{u_x R_0}{\Gamma_0} \ll \phi^{3/5}. \tag{38}$$

These forms come into alignment using asymptotic matching when $u_x \propto a^{3/5}$. Of particular note, we see here that the width of the core scales as $\phi^{3/5}$. Contrasting these last two equations with the Gaussian distribution Eq. (35), it is clear that Eqs. (37) and (38) are only valid when $\phi \ll 1$; that is, even though Eq. (38) resembles a Gaussian distribution, it is completely different from the Gaussian Eq. (35) in the large ϕ limit. Moreover, the tail distribution Eq. (37) contributes heavily to the energy $\mu\mathcal{E}_1$, which therefore cannot be deduced from the width of Eq. (38).

The $-8/3$ power law in Eq. (37) does not persist for arbitrarily large u_x, and in fact one can show using an argument similar to that in Sec. IV A that $p_{U_x}(u_x) \propto |u_x|^{-5}$ as $|u_x| \to \infty$ due to the singular behavior of a vortex ring at $\rho = R_0$ and $t = 0$. Including the large u behavior in our calculations changes the distribution from a stable distribution to a truncated stable distribution, which has finite second moment (and thus finite energy). This observation explains the seemingly inconsistent large and small ϕ approximations for $p_{U_x}(u_x)$ of a Gaussian and a stable distribution, respectively. The transition from a truncated stable distribution to a Gaussian distribution occurs near a volume fraction where the width of the core region is on the same order of magnitude as the cutoff, which follows immediately from the Berry–Esséen theorem [52]. For further discussion of the relative contributions of the core and the tails to the energy, both with and without truncation, see Appendix C.

C. Comparison with numerical simulations

Since a number of approximations were used to derive the distributions in the previous section, a comparison with numerical simulations is in order. In particular, in computing Eq. (34) we inserted a cutoff between the $-8/3$ and -5 power laws, and the use of Eq. (36) is not valid for small k.

Our numerical investigation involves a Monte Carlo integration of Eq. (28): we simulate the suspension by generating and evolving vortex rings uniformly in time and space in a spherical volume of radius $L = 100R_0$ for $t \in [0,\tau]$ with $\tau = 100R_0^2/\nu$ and computing the velocity at the origin. We fix the initial single-vortex circulation to be $\Gamma_0 = 100\nu$, so all the vortices have the same initial strength. The velocity field due to individual vortices is obtained by differentiating the streamfunction Eq. (4b) using a fourth-order-accurate finite-difference approximation. The velocity fields of individual vortices are then superimposed linearly to generate the total velocity field. This is a reasonable approximation in the dilute regime, $\phi \ll 1$, when vortices stay far enough apart so that they do not significantly interact.

Because of the special functions and the oscillatory integrand, the streamfunction Ψ is prohibitively expensive to evaluate directly. We compute it for several points on two overlapping grids and form a cubic spline interpolant to evaluate it at arbitrary points in space. One grid covers $\rho, |z| \leqslant 20R_0$ and $0 \leqslant t \leqslant 20R_0^2/\nu$ with 200^3 grid points, while another grid with higher resolution covers $0.75R_0 \leqslant \rho \leqslant 1.25R_0$, $|z| \leqslant 0.25R_0$, and $0 \leqslant t \leqslant 0.5R_0^2/\nu$, with $250^2 \times 100$ grid points around the initial singularity. For points outside these grids, Ψ is approximated using Eq. (5). Since the interpolated values of Ψ do not match Eq. (5) on the boundary of the grid, a buffer region is established where Ψ is represented as a convex combination of the interpolated value and Eq. (5); the smoothness of the transition is important to accurately compute the velocity. The integration required to compute Ψ in Eq. (4b) at any particular grid point is performed using a global adaptive quadrature (Matlab's integral function) with absolute and relative error tolerances 10^{-10} and 10^{-6}, respectively. A single simulation amounts to placing a random distribution of vortices, each with a

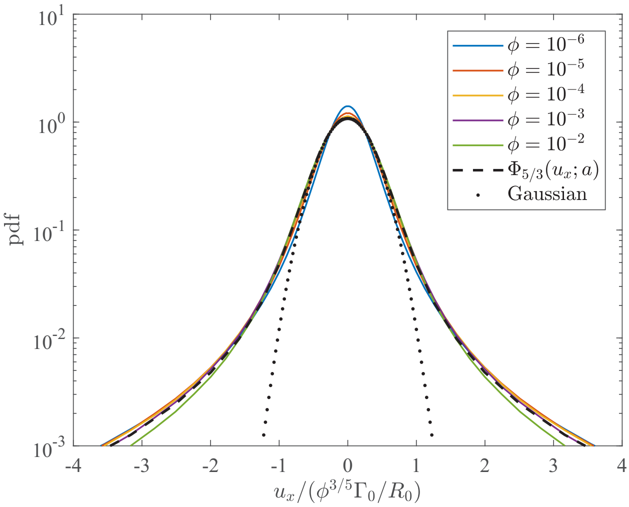

FIG. 6. The probability density function for the x-component of velocity (normalized by $\phi^{3/5}\Gamma_0/R_0$) for various ϕ. We see that the core scales with $\phi^{3/5}$. The dashed curve is the analytical expression $\Phi_{5/3}(u_x; a)$, which agrees closely with the numerics. The dotted curve is a Gaussian distribution with unit standard deviation, included for reference.

random position, orientation, and age, and using the machinery above to compute the velocity at the origin at that moment.

For a given value of the effective volume fraction $\phi = \mu R_0^5/\nu$ we run 15 million simulations on a distributed computing framework and then compute the probability density function $p_{U_x}(u_x)$ for a single component of velocity by placing the results in exponentially sized bins. Figure 6 shows this density normalized for a selection of different ϕ, along with the theoretical expression $\Phi_{5/3}(u_x; a)$ as a dashed line and a Gaussian distribution as a dotted line for reference. The numerical simulations appear to confirm the accuracy of this analytic estimate for the entire range of ϕ considered. Note in particular the scaling of the core width as $\phi^{3/5}$. Figure 7 shows the same distributions on a log-log scale, with a dashed line of slope $-8/3$ included for reference. The probability density function decays as $|u_x|^{-8/3}$ outside the core, as predicted in Eq. (37). We were unable to verify the predicted $|u_x|^{-5}$ power law for very large velocities due to the extreme resolution needed near the initial vortex filaments to properly capture the largest velocities.

For large enough velocities, the nearest vortex ring determines the velocity at a point, so that the many-vortex probability distribution $p_{U_x}(u_x)$ has the same tails as the single-vortex $p_{U_x^1}(u_x)$. In particular, outside the core of the distribution we have

$$p_{U_x}(u_x) \sim \phi\, p_{U_x^1}(u_x) = \phi \int_{|u_x|}^{\infty} \frac{p_{U^1}(u)}{2u}\, du, \qquad \frac{u_x R_0}{\Gamma_0} \gg \phi^{3/5}. \tag{39}$$

Figure 8 compares Eq. (39) (dashed curve) with PDFs divided by ϕ for several values of ϕ. There is excellent agreement outside the core of the distribution, so typical velocities in the suspension are indeed dominated by the nearest vortex ring except in the case of small velocities.

Figures 6–8 suggest strongly that $p_{U_x}(u_x)$ is a truncated stable distribution with smooth cutoff near $u_x \approx \pm 0.4\Gamma_0/R_0$. Note that this cutoff is independent of ϕ and only depends on the transition between small and large u asymptotics for the velocity distribution of a single vortex ring. When $\phi \ll 1$, the cutoff is far down the tail, so a stable distribution is a good approximation for the velocity distribution.

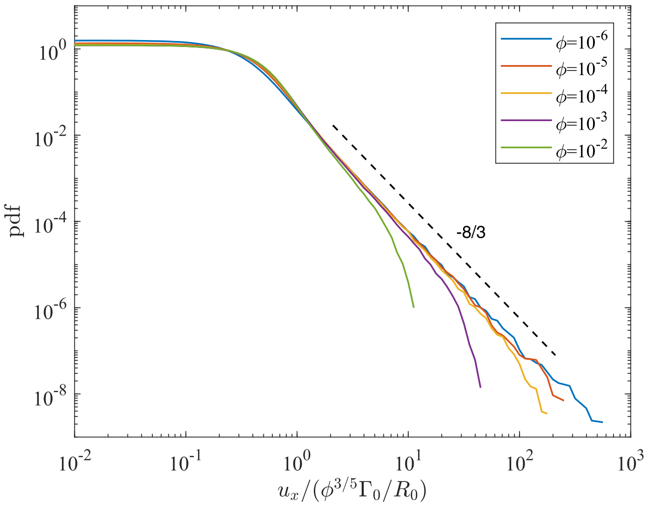

FIG. 7. The same distributions as in Fig. 6, but on a log-log scale. The additional dashed line verifies the $-8/3$ power law for large (but not very large) velocities.

V. ROBUSTNESS

In this section we consider the flow due to an arbitrary impulsive force localized near the origin in time and space and find the same far-field behavior as in the previous section. Thus, the analysis from the last section (except for the large-velocity $|u_x|^{-5}$ tails, which are specific to the vortex model) is generic and carries through to more general flows.

Various aspects of the flow due to an impulsive force have been studied in many contexts [21,45,53–55]. We follow a combination of Saffman [54] and Bühler [55]. Consider an external

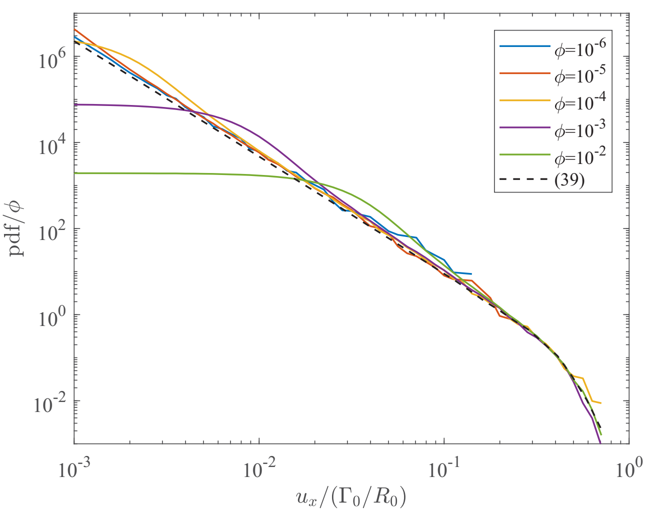

FIG. 8. Plot of the (normalized) probability density function for the x component of velocity divided by ϕ compared with Eq. (39) (the dashed line), showing close agreement, except at small velocities. In particular, regardless of ϕ, the distributions transition away from the $-8/3$ power law at around $u_x \approx 0.4\Gamma_0/R_0$, regardless of ϕ.

force density

$$\widetilde{\boldsymbol{F}}(\boldsymbol{r},t) = \rho_0\,\boldsymbol{F}(\boldsymbol{r})\,\frac{1}{\Delta t}\,g(t/\Delta t), \tag{40}$$

where ρ_0 is the constant fluid density, $g(s)$ is nonnegative with unit integral and with support contained in [0,1], and $\boldsymbol{F}(\boldsymbol{r})$ has compact support encompassing the origin. For small Δt, a classical argument (see, for example, Lamb [53] or Bühler [55]) shows that the nonlinear terms in the incompressible Navier–Stokes equations are negligible when considering the evolution due to this force of a fluid initially at rest. The pressure $\tilde{p}$ then satisfies a Poisson equation $\nabla^2\tilde{p} = \nabla\cdot\widetilde{\boldsymbol{F}}$ with boundary condition $\nabla\tilde{p}\to 0$ as $r\to\infty$. Bühler [55] concludes that $\tilde{p}$ has the same time dependence as $\widetilde{\boldsymbol{F}}$, i.e.,

$$\tilde{p}(\boldsymbol{r},t) = \rho_0\,p(\boldsymbol{r})\,\frac{1}{\Delta t}\,g(t/\Delta t). \tag{41}$$

The linear momentum equation can be integrated over $t\in[0,\Delta t]$, at the end of which

$$\boldsymbol{v}(\boldsymbol{r},\Delta t) + \nabla p(\boldsymbol{r}) = \boldsymbol{F}(\boldsymbol{r}), \tag{42}$$

where we neglected the viscous term since it is of order Δt after integration. Far away from the origin, the pressure is harmonic with

$$p(\boldsymbol{r}) \sim \frac{\boldsymbol{I}\cdot\boldsymbol{r}}{4\pi r^3}, \quad r\to\infty, \quad \text{where} \quad \boldsymbol{I} = \int_{\mathbb{R}^3}\boldsymbol{F}(\boldsymbol{r})\,dV, \tag{43}$$

so that $\rho_0\boldsymbol{I}$ is the total impulsive momentum input [55]. Substituting Eq. (43) into Eq. (42), we find that $v(\boldsymbol{r},\Delta t) = O(r^{-3})$ in the far field. In fact, for $\boldsymbol{I} = \pi\Gamma_0 R_0^2\hat{\boldsymbol{z}}$, the hydrodynamic impulse for the model vortex ring, the velocity $\boldsymbol{v}(\boldsymbol{r},\Delta t)$ found here exactly matches the $\xi\gtrsim 1$ limit of Eq. (7).

Similarly, we can determine the velocity distribution for long times knowing only the impulse (see, for example, Phillips [21] or Saffman [45]). Taking the curl of Eq. (42) gives vorticity $\boldsymbol{\omega}(\boldsymbol{r},\Delta t) = \nabla\times\boldsymbol{F}(\boldsymbol{r})$. Note that $\boldsymbol{\omega}(\boldsymbol{r},\Delta t)$ has compact support contained in the support of $\boldsymbol{F}$. Assume small Reynolds number, in this section defined to be $\mathrm{Re} := R_0F/\nu$, where F is a characteristic magnitude of $\boldsymbol{F}$ and R_0 is the radius of the smallest ball containing the support of $\boldsymbol{F}$. Then the nonlinear term in Navier–Stokes can be neglected, so the vorticity obeys a heat equation

$$\frac{\partial\boldsymbol{\omega}}{\partial t} \approx \nu\nabla^2\boldsymbol{\omega}, \quad t > \Delta t, \quad \boldsymbol{\omega}(\boldsymbol{r},\Delta t) = \nabla\times\boldsymbol{F}(\boldsymbol{r}). \tag{44}$$

In the limit $\Delta t\to 0$, this has solution

$$\boldsymbol{\omega}(\boldsymbol{r},t) = \frac{1}{(4\pi\nu t)^{3/2}}\int_{|\boldsymbol{r}'|\leqslant R_0}[\nabla\times\boldsymbol{F}(\boldsymbol{r}')]\,e^{-|\boldsymbol{r}'-\boldsymbol{r}|^2/4\nu t}\,dV_{\boldsymbol{r}'}. \tag{45}$$

For $\nu t \gg R_0\max(R_0,|\boldsymbol{r}|)$, we can expand the exponential to obtain

$$\boldsymbol{\omega}(\boldsymbol{r},t) = \frac{1}{(4\pi\nu t)^{3/2}}\int_{|\boldsymbol{r}'|\leqslant R_0}[\nabla\times\boldsymbol{F}(\boldsymbol{r}')]\,e^{-|\boldsymbol{r}|^2/4\nu t}\left(1 - \frac{|\boldsymbol{r}'|^2 - 2\boldsymbol{r}\cdot\boldsymbol{r}'}{4\nu t} + \cdots\right)dV_{\boldsymbol{r}'}. \tag{46}$$

The integral of the first term in the series vanishes; the next order term gives the asymptotic behavior of the vorticity:

$$\boldsymbol{\omega}(\boldsymbol{r},t) \sim \frac{\pi}{(4\pi\nu t)^{5/2}}\,e^{-|\boldsymbol{r}|^2/4\nu t}\int_{|\boldsymbol{r}'|\leqslant R_0}[\nabla\times\boldsymbol{F}(\boldsymbol{r}')](2\boldsymbol{r}\cdot\boldsymbol{r}' - |\boldsymbol{r}'|^2)\,dV_{\boldsymbol{r}'}, \quad \nu t \gg R_0\max(R_0,|\boldsymbol{r}|). \tag{47}$$

An integration by parts simplifies the expression:

$$\boldsymbol{\omega}(\boldsymbol{r},t) = \frac{2\pi}{(4\pi\nu t)^{5/2}}\, e^{-|\boldsymbol{r}|^2/4\nu t} \int_{|\boldsymbol{r}'|\leqslant R_0} \boldsymbol{F}(\boldsymbol{r}') \times (\boldsymbol{r}-\boldsymbol{r}')\, dV_{\boldsymbol{r}'}$$
$$= \frac{2\pi}{(4\pi\nu t)^{5/2}}\, e^{-|\boldsymbol{r}|^2/4\nu t} (\boldsymbol{I}\times\boldsymbol{r} - \boldsymbol{J}), \tag{48}$$

where

$$\boldsymbol{J} := \int_{|\boldsymbol{r}'|\leqslant R_0} \boldsymbol{F}(\boldsymbol{r}') \times \boldsymbol{r}'\, dV_{\boldsymbol{r}'}. \tag{49}$$

The corresponding velocity field can be found via the Biot–Savart law:

$$\boldsymbol{v}(\boldsymbol{r},t) = \frac{1}{2(4\pi\nu t)^{5/2}} \int_{\mathbb{R}^3} \frac{(\boldsymbol{I}\times\boldsymbol{r}_0 - \boldsymbol{J})\times(\boldsymbol{r}-\boldsymbol{r}_0)}{|\boldsymbol{r}-\boldsymbol{r}_0|^3}\, e^{-|\boldsymbol{r}_0|^2/4\nu t}\, dV_{\boldsymbol{r}_0}. \tag{50}$$

As $t \to \infty$, a vanishingly small error is introduced replacing $\boldsymbol{r}_0$ by $\boldsymbol{r}-\boldsymbol{r}_0$ in the exponential. Then

$$\boldsymbol{v}(\boldsymbol{r},t) \sim \frac{1}{2(4\pi\nu t)^{5/2}} \int_{\mathbb{R}^3} \frac{[\boldsymbol{I}\times(\boldsymbol{r}_0-\boldsymbol{r}) + (\boldsymbol{I}\times\boldsymbol{r}-\boldsymbol{J})]\times(\boldsymbol{r}-\boldsymbol{r}_0)}{|\boldsymbol{r}-\boldsymbol{r}_0|^3}\, e^{-|\boldsymbol{r}-\boldsymbol{r}_0|^2/4\nu t}\, dV_{\boldsymbol{r}_0}$$
$$= \frac{\boldsymbol{I}}{12(\pi\nu t)^{3/2}}. \tag{51}$$

This matches the $\xi \lesssim 1$ limit of Eq. (7) perfectly for the hydrodynamic impulse for the model vortex ring.

So we see that in the limit as $r \to \infty$, the velocity decays as $O(r^{-3})$, and for any fixed location, the velocity decays as $O(t^{-3/2})$ as $t \to \infty$. The transition between these two regimes occurs along the same viscous front as we have already analyzed for the vortex ring ($\xi = 1$). Indeed, Eq. (7) is a good approximation for the velocity away from the impulse for any flow due to a localized impulsive force. Therefore, all our analysis from the previous section carries through and so $\Phi_{5/3}(u_x; a)$ is an excellent approximation of the velocity distribution for a volume of fluid containing any swimmers that exert force in short bursts, such as for instance copepods [56,57].

VI. DISCUSSION

We analyzed the flow field of a model viscous vortex ring and found that for a flow which is initially a vortex filament, the absolute moments of velocity M_n are finite only for $\frac{5}{3} < n < 4$. Consistent with this observation, the density function of the magnitude of velocity is asymptotic to $u^{-8/3}$ for small velocities, and to u^{-5} for large velocities. The former power law is due to the long-time diffusion of vorticity as the vortex ring expands, while the latter is due to the initial diffusion of vorticity away from the vortex filament immediately after its formation. While the large u distribution will depend heavily on the exact model used (e.g., Min *et al.* [44] found exponential tails in their study of two-dimensional patches of vorticity because each isolated patch had a maximum velocity), the $u^{-8/3}$ power law for small velocities is robust in the sense that any flow brought about by an initial impulse will produce a distribution with the same power law.

We have constructed a model suspension of viscous vortex rings with convenient analytic properties by superimposing the flow fields for individual vortex rings positioned and oriented randomly throughout space and time. The velocity fluctuations were shown both analytically and numerically to fit a truncated stable distribution with tails decaying as $u^{-8/3}$. This distribution has core width proportional to $\phi^{3/5}$ but energy proportional to ϕ, the vortex volume fraction, so that most of the energy comes from the tail of the distribution (associated with large velocities). Points in space corresponding to the distribution's tail are only influenced by the nearest vortex ring, so interactions between vortices play a negligible role. However, with increasing volume fraction ϕ, the dominant contribution begins to come from the core region encompassing the far-field velocity of many not-so-distant vortices.

Our work extends efforts to understand the velocity fluctuations produced by swimmers at low Reynolds numbers to intermediate values. We expect the model to provide a good approximation for the flow fields associated with a variety of jellyfish species in a physically realistic regime of the Reynolds number ($60 \lesssim \mathrm{Re} \lesssim 2160$) [49], particularly in light of the robustness of the flow structure to perturbations of the initial impulse. Even among jellyfish, however, different types of flow fields are generated by different species: elongated jellyfish such as *Nemopsis bachei* generate a streak of vortex rings for efficient swimming [41,58], while more bulbous species like *Aurelia aurita* generate dual starting and stopping vortex rings (during power and recovery strokes) in the wake of the bell in a slower, axisymmetric-paddling locomotion [58–60]. The extent to which the distribution derived here remains appropriate for describing such systems, and related nonmotile systems, like pulsing corals [25], remains an open question for future exploration.

Finally, it is an open question whether the velocity distributions predicted here can be measured experimentally in some context. A realistic environment is probably too noisy to hope for the simple model presented here to have quantitative value, but possibly the tails of the distribution are robust enough to be measurable. Laboratory experiments are not out of the question, though a mechanism would need to be devised for adequate generation of the random vortices, in a tank large enough for edge effects to be negligible.

ACKNOWLEDGMENT

S.E.S. was supported partially by NSF Grant No. DMS-1661900.

APPENDIX A: MOMENTS OF THE VELOCITY OF A SINGLE VORTEX RING

In this section, we study the moments of the velocity field associated with a single vortex ring integrated over both time and space:

$$M_n := \int_0^\infty \int_V |\boldsymbol{v}|^n \, dV \, dt, \tag{A1}$$

where V is our domain, in this section taken to be $\mathbb{R}^3$. At the outset, it is not clear which moments exist, if any, and we shall see that many do not. To this end, we use Eq. (7) to approximate the far-field velocity and see that $|\boldsymbol{v}|$ decays like r^{-3} (where $r = \sqrt{z^2 + \rho^2}$) as $r \to \infty$ given any fixed time. Upon integrating over space, we therefore have that

$$\int_V |\boldsymbol{v}|^n \; dV = \int_V |\boldsymbol{v}|^n r^2 \, dr \, d\Omega \tag{A2}$$

is infinite for $2 - 3n \geqslant -1$, where $d\Omega$ denotes integration over the unit sphere. Therefore, $M_n = \infty$ for all $n \leqslant 1$, and for $n > 1$, the approximation Eq. (7) enables us to compute the integral explicitly. Asymptotically, we find that

$$\int_V |\boldsymbol{v}|^n \; dV = O(\Gamma_0^n (\nu t)^{3(1-n)/2}), \tag{A3}$$

valid as $t \to \infty$.

Another possible source of moment divergence lies at time $t = 0$, when the velocity field is singular at the vortex filament. For small times, the evolution of vorticity near a point on the vortex ring may be studied using a line vortex approximation. Consider therefore a line vortex located at the origin; the vorticity ζ is the Green's function for the heat equation multiplied by the initial circulation:

$$\zeta = \frac{\Gamma_0}{4\pi \nu t} \exp\left(-\frac{x^2 + y^2}{4\nu t}\right). \tag{A4}$$

Then the swirl velocity is

$$v = \frac{\Gamma_0}{2\pi\sqrt{x^2+y^2}}\left[1-\exp\left(-\frac{x^2+y^2}{4\nu t}\right)\right], \tag{A5}$$

counterclockwise around the origin. The velocity decays exponentially quickly far away, so we only need consider the near field (out to a distance proportional to $\sqrt{4\nu t}$) when determining the spatial moments. Near the vortex, $v \approx \Gamma_0\sqrt{x^2+y^2}/8\pi\nu t$. Integrating, we find that

$$\int |\boldsymbol{v}|^n \, dA = O\big(\Gamma_0^n(\nu t)^{1-n/2}\big), \tag{A6}$$

valid as $t \downarrow 0$, is finite for all nonnegative n and strictly positive t, so the vortex filament does not contribute to any possible divergence of the spatial moment for any $n \geqslant 0$ (except for possibly at the single time $t = 0$).

Looking across the entirety of the spatial domain, the arguments above suggest the existence of the spatial moments $\int_V |\boldsymbol{v}|^n \, dV$ at all positive t for all $n > 1$, but we are particularly interested in the moments M_n, which are integrals over both space and time. Examining the rate of decay of Eq. (A3) for large times results in infinite moment M_n precisely when $3(1-n)/2 \geqslant -1$, or $n \leqslant \frac{5}{3}$. Similarly, the behavior of Eq. (A6) at small times results in infinite moment M_n when $1 - n/2 \leqslant -1$, or $n \geqslant 4$. Thus, *the moments of* $\boldsymbol{v}$ *exist only for* $\frac{5}{3} < n < 4$.

APPENDIX B: THE PROBABILITY DENSITY FUNCTION FOR SINGLE VORTEX RING

For $\xi \leqslant 1$, the velocity is only a function of time ($t = (\Gamma_0 R_0^2/12u\sqrt{\pi}\nu^{3/2})^{2/3}$), so

$$\begin{aligned}\int_{v(\boldsymbol{r},t)=u,\,\xi\leqslant 1} \frac{dS_{\boldsymbol{r},t}}{|\nabla_{(\boldsymbol{r},t)} v(\boldsymbol{r},t)|} &= \frac{4}{3}\pi(4\nu t)^{3/2}\left(\frac{\Gamma_0 R_0^2}{8\sqrt{\pi}\nu^{3/2}t^{5/2}}\right)^{-1}\Bigg|_{t=(\Gamma_0R_0^2/12u\sqrt{\pi}\nu^{3/2})^{2/3}} \\ &= \frac{2^{8/3}\pi^{1/6}}{3^{11/3}}\frac{\Gamma_0^{5/3}R_0^{10/3}}{\nu}u^{-8/3}.\end{aligned} \tag{B1}$$

The integral for $\xi \geqslant 1$ is somewhat more complicated. From Eq. (7), we see that

$$v = \frac{\Gamma_0 R_0^2}{r^3}\frac{\sqrt{1+3\cos^2\varphi}}{4} =: \frac{\Gamma_0 R_0^2}{r^3} f(\varphi), \tag{B2}$$

where φ is the angle from the positive z-axis. When the velocity is u, $r = (\Gamma_0 R_0^2 f(\varphi)/u)^{1/3}$. Then

$$\begin{aligned}&\int_{v(\boldsymbol{r},t)=u,\xi\geqslant 1} \frac{dS_{\boldsymbol{r},t}}{|\nabla_{(\boldsymbol{r},t)} v(\boldsymbol{r},t)|} \\ &\quad= \int_0^\pi \int_0^{r_u(\varphi)^2/4\nu}\left(\frac{u}{r_u(\varphi)}\sqrt{9+\frac{f'(\varphi)^2}{f(\varphi)^2}}\right)^{-1} 2\pi r_u(\varphi)\sqrt{r_u(\varphi)^2 + r_u'(\varphi)^2}\sin\varphi \, dt\, d\varphi,\end{aligned} \tag{B3}$$

where we have parameterized our surface in θ, φ, t and performed the integral over θ. The integral in Eq. (B3) can be computed analytically:

$$\begin{aligned}\frac{2\pi}{4\nu u}\int_0^\pi \frac{r_u(\varphi)^4\sqrt{r_u(\varphi)^2+r_u'(\varphi)^2}}{\sqrt{9f(\varphi)^2+f'(\varphi)^2}} f(\varphi)\sin\varphi\, d\varphi &= \frac{\pi}{6}\frac{\Gamma_0^{5/3}R_0^{10/3}}{\nu}u^{-8/3}\int_0^\pi f(\varphi)^{13/3}\sin\varphi\, d\varphi \\ &= 0.01453\frac{\Gamma_0^{5/3}R_0^{10/3}}{\nu}u^{-8/3}.\end{aligned} \tag{B4}$$

APPENDIX C: ENERGY CONTRIBUTIONS FROM SECTIONS OF THE PDF

The expected energy of the suspension of vortices is

$$\langle E\rangle = \frac{3}{2}\int_{-\infty}^{\infty} u_x^2\, p_{U_x}(u_x)\, du_x. \tag{C1}$$

Equations (37) and (38) cannot be used by themselves to approximate the energy, since this results in divergence in the expression above, so the $|u_x|^{-5}$ tails for the largest velocities must be included to obtain a convergent integral.

Using Eqs. (37) and (38) to determine the behavior of the inner and middle regions, we find that

$$p_{U_x}(u_x) \approx \begin{cases} 0.2844a^{-3/5}\exp\left(-u_x^2/3.198a^{6/5}\right) & |u_x| \leqslant 3.260a^{3/5}, \\ 0.2395a|u_x|^{-8/3} & 3.260a^{3/5} \leqslant |u_x| \leqslant c, \\ 0.2395ac^{7/3}|u_x|^{-5} & |u_x| \geqslant c, \end{cases} \tag{C2}$$

where $c \approx 0.4\Gamma_0/R_0$, as in Fig. 8, and $a = 0.1096\,(\Gamma_0/R_0)^{5/3}\phi$ [from Eq. (36)]. A comparison to Eq. (1) suggests that Eq. (C2) somewhat underestimates $p_{U_x}(u_x)$ around the transition at $|u_x| = 3.260a^{3/5}$.

Let $\langle E_{\rm C}\rangle$, $\langle E_{-8/3}\rangle$, and $\langle E_{-5}\rangle$ be the portions of the energy using the approximations of $p_{U_x}(u_x)$ in the core (C), middle $(-8/3)$, and outer (-5) regions in Eq. (C2) with the appropriate bounds, so that $\langle E\rangle = \langle E_{\rm C}\rangle + \langle E_{-8/3}\rangle + \langle E_{-5}\rangle$. We find the contributions

$$\langle E_{\rm C}\rangle = 1.980a^{6/5}, \tag{C3a}$$

$$\langle E_{-8/3}\rangle = -3.196a^{6/5} + 2.156ac^{1/3}, \tag{C3b}$$

$$\langle E_{-5}\rangle = 0.3593ac^{1/3}. \tag{C3c}$$

Without the underestimate of $p_{U_x}(u_x)$ in the transition between the core and middle regions, the $a^{6/5}$ terms above should cancel exactly (since the energy is known to scale with ϕ and a is linear in ϕ), which we verified using Eq. (1) directly and integrating numerically. The lack of exact cancellation is a symptom of our approximations in the transition region. Thus, a rough estimate of the energy is $\langle E\rangle \approx 2.515ac^{1/3} = 0.2031(\Gamma_0/R_0)^2\phi$, a slight overestimate of the exact expression in Eq. (22). Hence, we see that the greatest contribution to the energy comes from the middle region of the distribution for small ϕ. As ϕ increases, the largest contribution begins to come from the core region, which encompasses the far-field velocity of the vortices. The transition from the tails contributing most of the energy to the core doing so happens at about the same value of ϕ where the distribution changes shape from a $\frac{5}{3}$-stable distribution to a Gaussian, due to the core width approaching the value of the cutoff between the middle and outer regions of Eq. (C2), which is independent of ϕ.

---

[1] R. E. Caflisch and J. H. C. Luke, Variance in the sedimentation speed of a suspension, Phys. Fluids **28**, 759 (1985).

[2] H. Nicolai and B. Herzhaft, Particle velocity fluctuations and hydrodynamic self-diffusion of sedimenting non-Brownian spheres, Phys. Fluids **7**, 12 (1995).

[3] J. H. C. Luke, Decay of velocity fluctuations in a stably stratified suspension, Phys. Fluids **12**, 1619 (2000).

[4] P. J. Mucha, S.-Y. Tee, D. A. Weitz, B. I. Shraiman, and M. P. Brenner, A model for velocity fluctuations in sedimentation, J. Fluid Mech. **501**, 71 (2004).

[5] E. Guazzelli and J. Hinch, Fluctutations and instability in sedimentation, Annu. Rev. Fluid Mech. **43**, 97 (2011).
[6] J. Möller and T. Narayanan, Velocity Fluctuations in Sedimenting Brownian Particles, Phys. Rev. Lett. **118**, 198001 (2017).
[7] C. Dombrowski, L. Cisneros, S. Chatkaew, R. E. Goldstein, and J. O. Kessler, Self-Concentration and Large-Scale Coherence in Bacterial Dynamics, Phys. Rev. Lett. **93**, 098103 (2004).
[8] K. D. Drescher, R. E. Goldstein, N. Michel, M. Polin, and I. Tuval, Direct Measurement of the Flow Field Around Swimming Microorganisms, Phys. Rev. Lett. **105**, 168101 (2010).
[9] J. S. Guasto, K. A. Johnson, and J. P. Gollub, Oscillatory Flows Induced by Microorganisms Swimming in Two Dimensions, Phys. Rev. Lett. **105**, 168102 (2010).
[10] T. Ishikawa and T. J. Pedley, Diffusion of swimming model micro-organisms in a semi-dilute suspension, J. Fluid Mech. **588**, 437 (2007).
[11] T. Ishikawa, Suspension biomechanics of swimming microbes, J. Roy. Soc. Interface **6**, 815 (2009).
[12] K. C. Leptos, J. S. Guasto, J. P. Gollub, A. I. Pesci, and R. E. Goldstein, Dynamics of Enhanced Tracer Diffusion in Suspensions of Swimming Eukaryotic Microorganisms, Phys. Rev. Lett. **103**, 198103 (2009).
[13] I. Rushkin, V. Kantsler, and R. E. Goldstein, Fluid Velocity Fluctuations in A Suspension of Swimming Protists, Phys. Rev. Lett. **105**, 188101 (2010).
[14] P. T. Underhill, J. P. Hernandez-Ortiz, and M. D. Graham, Diffusion and Spatial Correlations in Suspensions of Swimming Particles, Phys. Rev. Lett. **100**, 248101 (2008).
[15] J. M. Yeomans, D. O. Pushkin, and H. Shum, An introduction to the hydrodynamics of swimming microorganisms, Eur. Phys. J. Special Topics **223**, 1771 (2014).
[16] Z. Lin, J.-L. Thiffeault, and S. Childress, Stirring by squirmers, J. Fluid Mech. **669**, 167 (2011).
[17] I. M. Zaid, J. Dunkel, and J. M. Yeomans, Lévy fluctuations and mixing in dilute suspensions of algae and bacteria, J. Roy. Soc. Interface **8**, 1314 (2011).
[18] I. Zaid and D. Mizuno, Analytical Limit Distributions from Random Power-Law Interactions, Phys. Rev. Lett. **117**, 030602 (2016).
[19] B. Delmotte, E. E. Keaveny, E. Climent, and F. Plouraboué, Simulations of Brownian tracer transport in squirmer suspensions, IMA J. Appl. Math. **84**, 680 (2018).
[20] J. L. Synge and C. C. Lin, On a statistical model of isotropic turbulence, Trans. R. Soc. Can. **37**, 45 (1943).
[21] O. M. Phillips, The final period of decay of nonhomogeneous turbulence, Math. Proc. Cambridge Philos. Soc. **52**, 135 (1956).
[22] P. G. Saffman, Vortex models of isotropic turbulence, Philos. Trans. R. Soc., A **355**, 1949 (1997).
[23] C. Hamlet, L. A. Miller, T. Rodriguez, and A. Santhanakrishnan, The fluid dynamics of feeding in the upside-down jellyfish, in *Natural Locomotion in Fluids and on Surfaces* (Springer, Berlin, 2012), pp. 35–51.
[24] M. Kremien, U. Shavit, T. Mass, and A. Genin, Benefit of pulsation in soft corals, Proc. Natl. Acad. Sci. USA **110**, 8978 (2013).
[25] J. E. Samson, N. A. Battista, S. Khatri, and L. A. Miller, Pulsing corals: A story of scale and mixing, Biomath **6**, 1712169 (2017).
[26] A. Villanueva, C. Smith, and S. Priya, A biomimetic robotic jellyfish (Robojelly) actuated by shape memory alloy composite actuators, Bioinspir. Biomimet. **6**, 036004 (2011).
[27] S. P. Colin, J. H. Costello, J. O. Dabiri, A. Villanueva, J. B. Blottman, B. J. Gemmell, and S. Priya, Biomimetic and live medusae reveal the mechanistic advantages of a flexible bell margin, PLoS One **7**, e48909 (2012).
[28] J. C. Nawroth, H. Lee, A. W. Feinberg, C. M. Ripplinger, M. L. McCain, A. Grosberg, J. O. Dabiri, and K. K. Parker, A tissue-engineered jellyfish with biomimetic propulsion, Nature Biotechnology **30**, 792 (2012).
[29] T. Maxworthy, The structure and stability of vortex rings, J. Fluid Mech. **51**, 15 (1972).
[30] B. Cantwell and N. Rott, The decay of a viscous vortex pair, Phys. Fluids **31**, 3213 (1988).
[31] S. K. Stanaway, B. J. Cantwell, and P. R. Spalart, A numerical study of viscous vortex rings using a spectral method, Tech. Rep. 101401 (NASA, 1988).
[32] K. Shariff and A. Leonard, Vortex rings, Annu. Rev. Fluid Mech. **24**, 235 (1992).

[33] P. G. Saffman, *Vortex Dynamics* (Cambridge University Press, Cambridge, UK, 1992).
[34] J. E. Cater, J. Soria, and T. T. Lim, The interaction of the piston vortex with a piston-generated vortex ring, J. Fluid Mech. **499**, 327 (2004).
[35] Y. Fukumoto and F. Kaplanski, Global time evolution of an axisymmetric vortex ring at low Reynolds numbers, Phys. Fluids **20**, 053103 (2008).
[36] Y. Fukumoto, Global time evolution of viscous vortex rings, Theor. Comput. Fluid Dyn. **24**, 335 (2010).
[37] J. O. Dabiri and M. Gharib, Fluid entrainment by isolated vortex rings, J. Fluid Mech. **511**, 311 (2004).
[38] J. O. Dabiri, Note on the induced Lagrangian drift and added-mass of a vortex, J. Fluid Mech. **547**, 105 (2006).
[39] S. C. Shadden, J. O. Dabiri, and J. E. Marsden, Lagrangian analysis of fluid transport in empirical vortex ring flows, Phys. Fluids **18**, 047105 (2006).
[40] I. Delbende and M. Rossi, The dynamics of a viscous vortex dipole, Phys. Fluids **21**, 073605 (2009).
[41] J. O. Dabiri, S. P. Colin, and J. H. Costello, Fast-swimming hydromedusae exploit velar kinematics to form an optimal vortex wake, J. Exp. Biol. **209**, 2025 (2006).
[42] P. Lévy, *Calcul des Probabilités* (Gauthier-Villars, Paris, 1925).
[43] W. Feller, *An Introduction to Probability Theory and Its Applications* (John Wiley & Sons, New York, 1971), Vol. 2.
[44] I. A. Min, I. Mezic, and A. Leonard, Lévy stable distributions for velocity and velocity difference in systems of vortex elements, Phys. Fluids **8**, 1169 (1996).
[45] P. G. Saffman, The velocity of viscous vortex rings, Stud. Appl. Math. **49**, 371 (1970).
[46] M. J. McHenry and J. Jed, The ontogenetic scaling of hydrodynamics and swimming performance in jellyfish Aurelia aurita, J. Exp. Biol. **206**, 4125 (2003).
[47] J. C. Nawroth and J. O. Dabiri, Induced drift by a self-propelled swimmer at intermediate Reynolds numbers, Phys. Fluids **26**, 091108 (2014).
[48] B. J. Gemmell, S. P. Colin, J. H. Costello, and J. O. Dabiri, Suction-based propulsion as a basis for efficient animal swimming, Nat. Commun. **6** (2015).
[49] N. J. Olesen, K. Frandsen, and H. U. Riisgaård, Population dynamics growth and energetics of jellyfish Aurelia aurita in a shallow fjord, Marine Ecol. Progr. Ser. **105**, 9 (1994).
[50] L. Hörmander, *The Analysis of Linear Partial Differential Operators I* (Springer-Verlag, Berlin, 1983).
[51] J.-L. Thiffeault, Distribution of particle displacements due to swimming microorganisms, Phys. Rev. E **92**, 023023 (2015).
[52] M. F. Shlesinger, Comment on Stochastic Process with Ultraslow Convergence to a Gaussian: The Truncated Lévy Flight, Phys. Rev. Lett. **74**, 4959 (1995).
[53] H. Lamb, *Hydrodynamics*, 6th ed. (Cambridge University Press, Cambridge, 1932).
[54] P. G. Saffman, The large-scale structure of homogeneous turbulence, J. Fluid Mech. **27**, 581 (1967).
[55] O. Bühler, Impulsive fluid forcing and water strider locomotion, J. Fluid Mech. **573**, 211 (2007).
[56] H. Jiang and J. R. Strickler, Copepod flow modes and modulation: A modeling study of the water currents produced by an unsteadily swimming copepod, Philos. Trans. Roy. Soc. Lond. B **362**, 1959 (2007).
[57] H. Jiang and T. Kiørboe, The fluid dynamics of swimming by jumping in copepods, J. Roy. Soc. Interface **8**, 1090 (2011).
[58] S. P. Colin and J. H. Costello, Morphology, swimming performance and propulsive mode of six co-occurring hydromedusae, J. Exp. Biol. **205**, 427 (2002).
[59] J. O. Dabiri, S. P. Colin, J. H. Costello, and M. Gharib, Flow patterns generated by oblate medusan jellyfish: Field measurements and laboratory analyses, J. Exp. Biol. **208**, 1257 (2005).
[60] A. P. Hoover, B. E. Griffith, and L. A. Miller, Quantifying performance in the medusan mechanospace with an actively swimming three-dimensional jellyfish model, J. Fluid Mech. **813**, 1112 (2017).